

A Bayesian Approach to Forecasting Solar Cycles Using a Fokker–Planck Equation

P.L. Noble · M.S. Wheatland¹ ·

© Springer ●●●

Abstract A Bayesian method for forecasting solar cycles is presented. The approach combines a Fokker–Planck description of short–timescale (daily) fluctuations in sunspot number (Noble and Wheatland, 2011, *Astrophys. J.* **732**, 5) with information from other sources, such as precursor and/or dynamo models. The forecasting is illustrated in application to two historical cycles (cycles 19 and 20), and then to the current solar cycle (cycle 24). The new method allows the prediction of quantiles, *i.e.* the probability that the sunspot number falls outside large or small bounds at a given future time. It also permits Monte Carlo simulations to identify the expected size and timing of the peak daily sunspot number, as well as the smoothed sunspot number for a cycle. These simulations show how the large variance in daily sunspot number determines the actual reliability of any forecast of the smoothed maximum of a cycle. For cycle 24 we forecast a maximum daily sunspot number of 166 ± 24 , to occur in

¹Sydney Institute for Astronomy,
School of Physics,
The University of Sydney,
Sydney NSW 2006,
Australia
email: p.noble@physics.usyd.edu.au

March 2013, and a maximum value of the smoothed sunspot number of 66 ± 5 , indicating a very small solar cycle.

Keywords: Solar Cycle, Models; Sunspots, Statistics

1. Introduction

The solar cycle is the semi-periodic change in the level of magnetic activity on the Sun, driven by a cyclical change in the Sun's local magnetic field. The International Sunspot Number², defined as

$$s = k(10g + N), \quad (1)$$

where g is the number of sunspot groups, N is the number of individual spots, and k is a correction factor, is the most commonly used measure of solar activity (Bruzek and Durrant, 1977). Variation in the sunspot number is comprised of the semi-regular 11 year cycle, as well as large daily, weekly, and yearly fluctuations on top of the underlying secular variation (Abreu *et al.*, 2008; Noble and Wheatland, 2011).

The sunspot number is an important indicator of solar activity, and hence of the space weather experienced on the Earth (Petrovay, 2010). As a result reliable prediction of the sunspot number is important. There are several methods for forecasting sunspot numbers (see Petrovay, 2010; Kane, 2007; Pesnell, 2008 for reviews), including precursor methods, time-series methods, and dynamo model based methods. Precursor methods correlate aspects of a future solar cycle (*e.g.* sunspot maximum) with indices of current solar and geomagnetic activity. Time-series methods extrapolate sunspot data into the future using mathematical or statistical techniques, including nonlinear models (*e.g.*

²Sunspot data are provided by the US National Geophysical Data Center (NGDC) at <http://www.ngdc.noaa.gov/stp/spaceweather.html>.

Aguirre, Letellier, and Maquet, 2008; Hanslmeier and Brajša, 2010; and Letellier *et al.*, 2006), statistical techniques (*e.g.* Akaike, 1978; Yule, 1927; Allen and Huff, 2010), and neural networks (*e.g.* Conway, 1998). Physical predictions are provided by dynamo-based models, which start with models of the Sun’s internal dynamo, the source of the magnetic fields of sunspots (*e.g.* Dikpati and Gilman, 2006; Dikpati, de Toma, and Gilman, 2006). Precursor, time series, and dynamo-based methods all forecast solar activity with some success (Hathaway, 2009), with precursor methods being the most successful (Kane, 2007).

Two specific criticisms of existing approaches to prediction are that it is difficult to rigorously combine forecasts from the competing methods, and that it is unclear how to update and/or reconcile forecasts (in particular long-range precursor forecasts) with new sunspot data as it becomes available. These problems were addressed by Hathaway, Wilson, and Reichmann (1999), who used precursor methods to forecast the size of the underlying cycle and then regressions to update precursor forecasts as new data became available. In this paper we also present an approach to prediction which combines precursor and time-series methods. Our method is similar to that of Hathaway, Wilson, and Reichmann (1999), with some specific differences. We combine sunspot data with precursor forecasts in a statistically rigorous way using a Bayesian framework, rather than combining methods using weighted averages. We also forecast the short time-scale fluctuations in sunspot number (*e.g.* the variance in the daily sunspot number), in addition to the size and shape of the underlying solar cycle.

Section 2 covers the theory of the Bayesian approach to forecasting daily sunspot numbers. Section 2.1 introduces the Fokker–Planck model used to describe the distribution of sunspot numbers, and Section 2.2 gives the details of the Bayesian method. Section 2.3 discusses the historical average solar cycle, or ‘mean cycle’, which we use as a starting point for prediction. Section 2.4 introduces a Monte–Carlo approach to simulating daily sunspot numbers based on analytic approximations to the Fokker–Planck model, which permits analysis

of the size and shape of the average underlying solar cycle, as well as construction of the joint distribution of the size and timing of maximum daily sunspot number. We also show how the large variance in daily sunspot number results in large variance in the monthly smoothed maximum sunspot number $\langle R \rangle_{\text{max}}$, and discuss the implications of this for the reliability of any forecast of the maximum of the cycle. Section 3 illustrates the Bayesian framework from Section 2 in application to two historical solar cycles, namely cycle 19 (in Section 3.1) and cycle 20 (in Section 3.2). Section 4 applies the Bayesian method to forecast the current cycle (cycle 24). Techniques from Section 2 are used to quantify the size of large/small sunspot numbers during cycle 24, and to estimate the likely size and timing of the next maximum in both daily sunspot number, and monthly smoothed sunspot number $\langle R \rangle_{\text{max}}$.

2. A Bayesian Approach to Solar Cycle Forecasting

2.1. Fokker–Planck Model for Sunspot Number

The solar cycle variation in sunspot number comprises long-term secular variation, and large short-term statistical fluctuations. The long-term variation may be considered the underlying solar cycle, driven by the internal dynamo, and the short-term fluctuations attributed to complicated physical processes on the solar surface associated with sunspot formation, evolution and dispersion (Parker, 1955).

The long-term solar cycle variation over a single cycle may be described by a cycle amplitude, cycle period, and cycle asymmetry (Hathaway, Wilson, and Reichmann, 1994), which we represent with a ‘driver function’ $\theta(t)$. For illustrative purposes we consider first the simple choice for $\theta(t)$ of harmonic variation:

$$\theta(t) = \alpha_0 + \alpha_1 \sin(2\pi t/\alpha_2 + \alpha_3), \quad (2)$$

where α_1 is the cycle amplitude, $\alpha_2 \approx 11$ years is the cycle period and α_3 is the cycle phase. With this choice there is no cycle asymmetry.

Short-term fluctuations in sunspot number on top of the driver function $\theta(t)$ may be modelled using a probability distribution function $f(s, t) = f(s, t|s_0, t_0)$, such that $f(s, t)ds$ is the probability that the sunspot number is between s and $s + ds$ at time t . This approach represents the sunspot number as a continuous random variable. Noble and Wheatland (2011) modelled the time evolution of $f(s, t)$ using the Fokker–Planck equation:

$$\frac{\partial f}{\partial t} = \frac{1}{2} \frac{\partial^2}{\partial s^2} [\sigma^2(s, t)f(s, t)] - \frac{\partial}{\partial s} [\mu(s, t)f(s, t)], \quad (3)$$

where $\mu(s, t)$ describes deterministic changes in sunspot number, and $\sigma^2(s, t)$ is a variance describing stochastic variation. Sunspot number is non-negative, so the appropriate boundary condition at $s = 0$ is a ‘zero probability flux’ condition

$$\mu(s, t)f(s, t) - \frac{1}{2} \frac{\partial}{\partial s} [\sigma^2(s, t)f(s, t)] \Big|_{s=0} = 0. \quad (4)$$

An appropriate choice for $\mu(s, t)$, in terms of the driver function $\theta(t)$ is

$$\mu(s, t) = \kappa [\theta(t) - s]. \quad (5)$$

This choice causes the fluctuating sunspot numbers to tend to return to the value $\theta(t)$ with a characteristic timescale $1/\kappa$. In this way the driver function $\theta(t)$ represents the secular or long-term sunspot number.

The size of the observed squared deviations $r^2(t) = [s(t) - s(t - \Delta t)]^2$, a proxy for daily sunspot number variance, tends to increase with sunspot number (Noble and Wheatland, 2011). Therefore a simple choice for the variance, which models this increase is

$$\sigma^2(s, t) = \beta_0 + \beta_1 s + \beta_2 s^2, \quad (6)$$

where β_0 describes variance in sunspot number at $s = 0$, and β_1 and β_2 describe the increase in variance with sunspot number (we assume that β_0, β_1 and β_2 are all positive or zero). The model then has four parameters $(\kappa, \beta_0, \beta_1, \beta_2)$, together with any parameters in the driver function $\theta(t)$.

The choices of Equations (4), (5) and (6) are discussed in detail in Noble and Wheatland (2011). The authors showed that the model given by Equations (2) to (6) applied to historical monthly sunspot number data generates a probability distribution function $f(s, t)$ which agrees both quantitatively and qualitatively with observed sunspot statistics, even for the simple harmonic choice for $\theta(t)$. The model parameters were estimated from the historical data using a maximum likelihood procedure explained in Section 2.2.

A more realistic choice of driver function $\theta(t)$ for a single solar cycle than Equation (2) is provided by the functional form (Hathaway, Wilson, and Reichmann, 1994):

$$\theta(t) = \frac{a(t - t_0)^3}{\exp\left[-(t - t_0)^2/b^2\right] - c}, \quad (7)$$

where t_0 is the start of the cycle, and a, b and c represent the cycle amplitude, period, and asymmetry respectively. With this choice of driver function there are seven parameters in the Fokker–Planck model, which may be represented in a vector

$$\mathbf{\Omega} = [a, b, c, \kappa, \beta_0, \beta_1, \beta_2]. \quad (8)$$

The distribution of model sunspot numbers is written $f(s, t; \mathbf{\Omega})$ to indicate the explicit dependence of the distribution on the model parameters. We assume that the cycle start date t_0 is known, but it could be treated as another parameter and estimated from the data.

If the parameters $\mathbf{\Omega}$ generating sunspot data are known, the time evolution of the distribution of sunspot numbers $f(s, t; \mathbf{\Omega})$ is uniquely determined by the Fokker–Planck Equation (3). However, the parameters are unknown. To describe

historical sunspot numbers the parameters may be estimated from historical sunspot data, following Noble and Wheatland (2011) [who used Equation (2) as the choice of $\theta(t)$]. For forecasting, it is necessary to estimate values $\hat{\Omega}$ of the model to forecast future sunspot numbers. These procedures are explained in Section 2.2.

2.2. Bayesian Estimation of Model Parameters

Given an observed set $\mathbf{s} = \{s_0, s_1, \dots, s_T\}$ of sunspot numbers at times $\{t_0, t_1, \dots, t_T\}$, the maximum likelihood (ML) estimate is the parameter set $\hat{\Omega}$ which maximises the likelihood function representing the probability of the data given the model:

$$\mathcal{L}(\mathbf{s}|\Omega) = \prod_{i=1}^{i=T} f(s_i, t_i | s_{i-1}, t_{i-1}; \Omega). \quad (9)$$

We assume that the distribution of s_i at time t_i depends only on the previous observation s_{i-1} at time t_{i-1} , which is the Markov property (Karatzas and Shreve, 1988).

ML estimates are optimal in the sense that they are both efficient and consistent in large samples (Dacunha-Castelle and Florens-Zmirou, 1986). However, ML estimates are limited in that they only use information from the observed data, and ignore other information which may be available.

With sunspot data we have additional information about the possible size, shape, and length of a future solar cycle, which may be included in the forecast using the Bayesian method (*e.g.* Sivia, 2006). The additional information may be in the form of a dynamo-based forecast, or a precursor forecast, for a future cycle. Our confidence in the reliability of this information is represented by a ‘prior distribution’ $\mathcal{P}(\Omega)$ for the model parameters Ω given the information. For example, if a precursor forecast for the variance parameter β_0 is $\bar{\beta}_0$, and if the parameter β_0 is not correlated with other model parameters, then an appropriate

choice of a prior distribution for this parameter is

$$\mathcal{P}(\beta_0) = \frac{1}{\sqrt{2\pi\sigma_{\beta_0}^2}} \exp \left[-\frac{1}{2} \left(\frac{\beta_0 - \bar{\beta}_0}{\sigma_{\beta_0}} \right)^2 \right], \quad (10)$$

where the variance $\sigma_{\beta_0}^2$ represents how confident we are that β_0 coincides with $\bar{\beta}_0$.

Because we are dealing with multiple parameters which may be correlated, it is necessary to include possible correlations in the prior. For the choice of Gaussian-distributed priors it is appropriate to use the general multinormal distribution

$$\mathcal{P}(\boldsymbol{\Omega}) = \frac{1}{(2\pi)^{k/2} |\Sigma|^{1/2}} \exp \left[-\frac{1}{2} (\boldsymbol{\Omega} - \bar{\boldsymbol{\Omega}}) \Sigma^{-1} (\boldsymbol{\Omega} - \bar{\boldsymbol{\Omega}})' \right], \quad (11)$$

where k is the number of parameters in $\boldsymbol{\Omega}$, and the matrix Σ is the variance-covariance matrix describing the uncertainties in each parameter and the co-dependence of the parameters. For the parameters in the Hathaway, Wilson, and Reichmann (1994) driver function (Equation (7)), Σ is a 7×7 matrix of the form

$$\Sigma = \begin{pmatrix} \sigma_a^2 & \sigma_{a,b} & \cdots & \sigma_{a,\beta_2} \\ \sigma_{b,a} & \sigma_b^2 & \cdots & \sigma_{b,\beta_2} \\ \vdots & \vdots & \ddots & \vdots \\ \sigma_{\beta_2,a} & \sigma_{\beta_2,b} & \cdots & \sigma_{\beta_2}^2 \end{pmatrix}, \quad (12)$$

where σ_i^2 is the uncertainty in parameter i and $\sigma_{i,j}$ is the covariance between parameters i and j , for $i, j = a, b, \dots, \beta_2$. As an example of the importance of correlations, it is well known that cycles which rise rapidly tend to be large (Waldmeier, 1935), so that we expect parameters describing the period and amplitude to be negatively correlated.

Predictions incorporating prior information may then be made as follows. When a cycle begins, daily sunspot data $\mathbf{s} = \{s_0, s_1, \dots, s_T\}$ becomes available.

This can be combined with the prior information by calculating the ‘posterior distribution’ $\mathcal{P}(\boldsymbol{\Omega}|\mathbf{s})$, according to Bayes’ rule (Sivia, 2006):

$$\mathcal{P}(\boldsymbol{\Omega}|\mathbf{s}) = \frac{\mathcal{P}(\mathbf{s}|\boldsymbol{\Omega}) \mathcal{P}(\boldsymbol{\Omega})}{\mathcal{P}(\mathbf{s})}. \quad (13)$$

The term $\mathcal{P}(\mathbf{s}|\boldsymbol{\Omega})$ in Equation (13) is the likelihood function (9), and the denominator is a normalising constant. The posterior distribution combines information about $\boldsymbol{\Omega}$ contained in the data (the time series approach), with relevant information external to the data (*e.g.* from precursor and/or dynamo models, or any other source).

We are unable to solve the Fokker–Planck equation (3) analytically, so we cannot evaluate the likelihood $\mathcal{P}(\mathbf{s}|\boldsymbol{\Omega})$ in closed form. An analytic approximation appropriate for daily data is (Noble and Wheatland, 2011):

$$\begin{aligned} f(s, \tau|s_0; \boldsymbol{\Omega}) = & \frac{1}{\sqrt{2\pi\sigma^2(s_0, t_0)\tau}} \left[\exp \left\{ -\frac{[s - (s_0 + \mu(s_0, t_0)\tau)]^2}{2\sigma^2(s_0, t_0)\tau} \right\} \right. \\ & \left. + \exp \left\{ -\frac{[s + (s_0 + \mu(s_0, t_0)\tau)]^2}{2\sigma^2(s_0, t_0)\tau} \right\} \right], \end{aligned} \quad (14)$$

where $\tau = t - t_0$. Equation (14) is the conditional probability distribution function of the random variable $|s(t)|$, where $s(t)$ is a normal random variable with mean $s_0 + \mu(s_0, t_0)$ and variance $\sigma^2(s_0, t_0)\tau$, and s_0 is the sunspot number at time t_0 . Using this approximate solution, the likelihood function (9) is

$$\begin{aligned} \mathcal{P}(\mathbf{s}|\boldsymbol{\Omega}) = & (2\pi)^{-\left(\frac{T}{2}\right)} \prod_{i=1}^T \left[\exp \left\{ -\frac{[s_i - (s_{i-1} + \mu_{i-1}\tau)]^2}{2\sigma_{i-1}^2\tau} \right\} \right. \\ & \left. + \exp \left\{ -\frac{[s_i + (s_{i-1} + \mu_{i-1}\tau)]^2}{2\sigma_{i-1}^2\tau} \right\} \right], \end{aligned} \quad (15)$$

where $\mu_i = \mu(s_i, t_i)$ and $\sigma_i^2 = \sigma^2(s_i, t_i)$.

Given the posterior distribution $\mathcal{P}(\boldsymbol{\Omega}|\mathbf{s})$ a specific estimate for the parameters $\boldsymbol{\Omega}$ may be calculated in a number of ways (Jaynes and Bretthorst, 2003). In this

paper we use the the most probable, or ‘modal estimate’ of Ω :

$$\hat{\Omega} = \operatorname{argmax} \mathcal{P}(\Omega|\mathbf{s}). \quad (16)$$

2.3. Construction of a Mean Solar Cycle Prior

Rather than using a specific precursor forecast, we consider using an historical average solar cycle, which we refer to as a ‘mean cycle’, as a prior. This means that before the start of a cycle the most probable shape of the cycle (*i.e.* the parameters in the driver function) and the variance of the cycle (*i.e.* the parameters in $\sigma^2(s, t)$ of the coming cycle) are represented by an historical average. This choice may be interpreted as a ‘guess in total ignorance’.

To determine the parameters $\bar{\Omega}$ for the mean cycle we consider daily sunspot data for the previous 13 solar cycles over the interval 1850 to 2010. The Hathaway, Wilson, and Reichmann (1994) driver function given by Equation (7) is assumed to represent the shape of each underlying cycle, and the variance of each cycle is modelled by Equation (6). For each solar cycle maximum likelihood estimates $\hat{\Omega} = [\hat{a}, \hat{b}, \hat{c}, \hat{\kappa}, \hat{\beta}_0, \hat{\beta}_1, \hat{\beta}_2]$ of the seven model parameters are calculated, as shown in Table 1.

The average for each parameter over the previous 13 cycles is assumed to represent the mean cycle, and is used in our prior distribution. The sample means (denoted $\bar{\Omega}$) are given in Table 2. The variance–covariance matrix Σ is calculated using sample covariances between the ML estimates for the seven parameters in Table 1. For example the covariance between the amplitude a and period b in Σ is

$$\sigma_{a,b} = \frac{1}{12} \sum_{i=1}^{13} (\hat{a}_i - \bar{a})(\hat{b}_i - \bar{b}). \quad (17)$$

The (non-dimensional) correlation matrix is given in Table 3. A number of important correlations exist. In particular, the large correlation between κ and β_1 (89%) shows the strong relationship between the variance parameters and the rate at which sunspot number returns to the level $\theta(t)$. There are also significant

correlations between the size of the cycle a , and the time to maximum b and asymmetry c (collectively describing the Waldmeier Effect (Waldmeier, 1935)).

2.4. Fokker–Planck Modelling of the Mean Solar Cycle

In this section we investigate characteristics of the average solar cycle using the mean cycle parameters $\bar{\Omega}$ estimated from daily sunspot data over the interval 1850 to 2010, given in Table 2. The driver function Equation (7) with parameter values from Table 2 describes the average size and shape of the underlying solar cycle. Short-term deviations in sunspot number from this average are described by the three variance parameters in Table 2.

Figure 1 illustrates the mean cycle (*i.e.* the sunspot model with $\Omega = \bar{\Omega}$), and simulations of daily sunspot number over the mean cycle using the Fokker–Planck model. The red curve (solid) in Figure 1 is the Hathaway, Wilson, and Reichmann (1994) driver function $\theta(t)$, given by Equation (7) with mean cycle parameters \bar{a}, \bar{b} and \bar{c} . The maximum value of the driver function $\theta_{\max} = 119$ occurs 4.4 years after the cycle start date. To investigate the likely size of short-term deviations about the driver $\theta(t)$, we numerically solve the Fokker–Planck equation (3) for the initial condition $f(s_0, t_0; \bar{\Omega}) = \delta(s_0)$ with $s(t_0) = 0$ at $t_0 = 0$. The solution is obtained from $t = 0$ to $t = 11$ years. Based on the numerical solutions for $f(s, t|s_0, t_0; \bar{\Omega})$ we calculate the upper and lower 1% quantiles, which are the curves $s_U(t)$ and $s_L(t)$ defined by

$$\int_0^{s_L(t)} ds' f(s', t|s_0, t_0; \bar{\Omega}) = \int_{s_U(t)}^{\infty} ds' f(s', t|s_0, t_0; \bar{\Omega}) = 0.01. \quad (18)$$

These curves delineate boundaries of extreme sunspot numbers (*i.e.* the probability that the sunspot number is larger or smaller than $s_U(t)$ or $s_L(t)$ respectively, from a given initial condition is 1%). The blue curves (dot/dashed) in Figure 1 show these upper and lower 1% quantiles for the mean cycle. The maximum value attained by the upper 1% quantile is $s_U(t) = 234$, which occurs 4.3 years

after the start of the cycle. This means that on average solar maximum occurs 4.3 years after the start of the cycle, and that there is a 1% chance of observing a daily sunspot number larger than 234 at solar maximum for an average cycle, given $s(t_0) = 0$.

Using the analytic approximation (Equation (14)) we can simulate daily sunspot numbers over the mean cycle. To do this we repeatedly generate random variables $s(t)$ from the conditional probability distribution (Equation (14)) with parameter values from Table 2. These numbers represent a sequence of possible daily sunspot numbers (one Monte Carlo simulation). The green points in Figure 1 are an example of simulated daily sunspot numbers. The maximum daily sunspot number s^* for this particular simulation is $s^* = 266$, which occurs 4.4 years after the cycle begins. In this simulation 1.1% and 1.8% of the sunspot numbers are greater than and less than the upper and lower 1% quantiles respectively.

With the Fokker–Planck model we can investigate the likely size and timing of daily sunspot maximum using repeated Monte–Carlo simulations. We denote by t^* the time of the occurrence of the maximum s^* of the daily sunspot number, for one simulation. Figure 2 shows a Monte Carlo estimate of the joint distribution $f(s^*, t^* | s_0, t_0; \bar{\Omega})$ of the size and timing of daily sunspot maximum based on 5×10^5 simulations. Each simulation is generated in the same way as the single instance shown in Figure 1. The expected size of daily sunspot maximum (the average over the simulations) is $\langle s^* \rangle = 271$, which occurs approximately $\langle t^* \rangle = 4.4$ years after the start of the cycle. This is comparable to the sample average maximum sunspot number from the previous 13 cycles (see Section 2.3), which is 255. The largest value of the daily sunspot number of the 5×10^5 simulations is $s^* = 504$, which suggests that mean cycle can generate extremely large sunspot numbers, although it is very unlikely (the mean cycle is expected to generate one such event every 5×10^5 cycles, or 5 million years).

We can also investigate the monthly smoothed sunspot number $\langle R \rangle_{\max}$, which is the main focus of much of the existing literature (Petrovay, 2010). During each simulation of daily sunspot numbers discussed above, we calculate a 13-month boxcar average sunspot number $\langle R \rangle$, and store the size of the maximum $\langle R \rangle_{\max}$. Figure 3 plots the distribution of $\langle R \rangle_{\max}$ based on 5×10^5 simulations of daily sunspot number. The expected value over the simulations is $\langle R \rangle_{\max} = 125 \pm 8$, and the lower and upper 5% quantiles are 113 and 138 respectively. For comparison the average smoothed maximum from the previous 13 cycles is 121.

Figure 3 has important implications for any forecast of $\langle R \rangle_{\max}$. Even if the model parameters for a solar cycle are known, large daily variation in sunspot number causes large variation in the possible smoothed maximum value of the cycle. This indicates that the reliability of any forecast of $\langle R \rangle_{\max}$ is limited by the large daily fluctuations in sunspot number.

3. Forecasting Historical Solar Cycles

In the following sections we consider application of the model to forecasting two historical solar cycles: cycles 19 and 20. Cycle 19 is chosen because it is the largest solar cycle since daily sunspot number records began (Kane, 2002). In contrast, Cycle 20 is very similar in amplitude and shape to the mean cycle. As such these cycles are very different in size and shape, and useful as illustrations of the Bayesian forecasting method described in Section 2.2. The two cycles are shown in Figure 4. The maximum of the observed smoothed sunspot number for cycle 19 is 201, and the maximum for cycle 20 is 110.

In the forecasts in this section we use the mean cycle constructed in Section 2.3 as a prior, and then we make updated predictions using successively more historical data from the start of a cycle, to demonstrate the Bayesian prediction method from Section 2.2. We use the analytic approximation (Equation (14)) to

the solution to the Fokker–Planck equation to evaluate the likelihood function (15), and we use the mean cycle estimates discussed in Section 2.3 with the multivariate normal prior distribution (Equation (11)). Because $\mathcal{P}(\mathbf{s})$ in Bayes’ rule (13) is required only as a normalising constant, we calculate the posterior distribution $\mathcal{P}(\boldsymbol{\Omega}|\mathbf{s}) \propto \mathcal{P}(\mathbf{s}|\boldsymbol{\Omega})\mathcal{P}(\boldsymbol{\Omega})$, and evaluate the modal estimate $\hat{\boldsymbol{\Omega}}$ of Equation (16) by numerical determination of the location of the maximum of the posterior distribution.

3.1. Solar Cycle 19

Solar cycle 19, which occurred from 1954 to 1965, is the largest cycle on record. As such it provides a useful illustration of how forecasts starting from a prior consisting of the mean cycle are modified by observation of larger than expected sunspot numbers.

First we consider applying the Bayesian estimation procedure to sunspot data for the entire cycle. If we take the mean cycle as the prior and take all daily sunspot numbers from 1 January 1954 to 31 December 1964 as data \mathbf{s} , construction of the posterior $\mathcal{P}(\boldsymbol{\Omega}|\mathbf{s}) \propto \mathcal{P}(\mathbf{s}|\boldsymbol{\Omega})\mathcal{P}(\boldsymbol{\Omega})$ and estimation of parameters gives the modal estimates $\hat{\boldsymbol{\Omega}}$ in Table 4. The difference between the ML estimates in Table 1 and the Bayesian estimates in Table 4 is the influence of the prior distribution in the calculation of the posterior.

We can repeat the calculation using only part of the data from the start of cycle 19 as input in \mathbf{s} . By constructing the posterior repeatedly, using successively more data from the start of the cycle, we mimic the process of forecasting and updating the forecast. Figure 5 illustrates the process of successive forecasting for this cycle. The green points are the observed daily sunspot numbers for cycle 19. The driver function for the mean cycle (the prior for the forecasts) is shown in blue (dot/dash). The three black curves (solid) are the driver functions given by Equation (7) calculated using Bayesian model parameters estimated with different amounts of daily sunspot data. The black curve with the smallest

maximum value is obtained using ten days of data from the start of the cycle, the next smallest uses one year of data from the start of the cycle, and the black curve with the largest maximum value uses two years of data. The driver function corresponding to the final Bayesian estimate using all data for the cycle (which has a maximum of $\theta_{\max} = 182$) is shown by the red dashed curve. This figure shows how, as parameter estimates are updated with additional daily sunspot data, the size, period and asymmetry of the forecast of the underlying solar cycle changes. Initial estimates of the size of the sunspot maximum are lower than that of the mean cycle, but the large sunspot numbers observed from about 1956 onwards cause the estimates of the cycle maximum to increase.

Figure 6 shows the estimate of maximum smoothed sunspot number $\langle R \rangle_{\max}$ as a function of the time of the latest data used for the prediction. These estimates are calculated by averaging over 10^5 simulations (blue squares), as discussed in Section 2.4. The first estimate of $\langle R \rangle_{\max}$ is calculated using 10 days of data which consisted of 10 consecutive spotless days. The solid black curve is the expected value of $\langle R \rangle_{\max}$ calculated using all daily data for cycle 19. Early Bayesian estimates (*i.e.* using data from 1954 to 1955) of $\langle R \rangle_{\max}$ are small because the data is dominated by a large number of days early in the cycle with zero sunspot number. From 1955 onwards the sunspot numbers increase more rapidly than expected for the mean cycle. As a result the Bayesian result for $\langle R \rangle_{\max}$ rises rapidly until around 1958, and after that the estimate of $\langle R \rangle_{\max}$ is approximately constant, fluctuating between 180 and 195. The final estimate (*i.e.* the estimate using all daily sunspot data for cycle 19) is $\langle R \rangle_{\max} = 189 \pm 11$, corresponding to the parameters in Table 4. The observed value of $\langle R \rangle_{\max} = 201$ is shown by the black dashed line, and is roughly one standard deviation higher than the expected value, given the data. This difference illustrates the large variability in the cycle maximum possible due to the daily sunspot number fluctuations (see Section 2.4).

3.2. Solar Cycle 20

Solar cycle 20, which occurred from 1965 to 1976, is substantially different in character to cycle 19, discussed in Section 3.1. The shape of this cycle is more typical, similar to the mean cycle.

Following the approach in Section 3.1, we first consider Bayesian estimation applied to daily sunspot data for the entire cycle, using the mean cycle as a prior. The data span 1 January 1965 to 31 December 1976. Table 5 lists the model estimates $\hat{\Omega}$ for the Fokker–Planck model parameters obtained using the Bayesian procedure from Section 2.2 applied to the daily sunspot data for the whole cycle. The difference between the Bayesian and ML estimates is again due to the influence of the prior in the calculation of the posterior distribution.

Figure 7 illustrates predictions for cycle 20 following Figure 5. The green points are the observed daily sunspot numbers for cycle 20. The three black (solid) curves show the driver function (Equation (7)) calculated using successively more sunspot data. The black curve with the largest maximum is estimated using ten days of data from the start of the cycle, the next largest uses one year of data, and the third black curve uses two years of data. The driver function corresponding to the final Bayesian estimate (which has a maximum $\theta_{\max} = 124$) is shown by the red dashed curve. Initial estimates of the cycle amplitude are larger than that of the mean cycle, as indicated in Figure 7. The observation of many days with small sunspot numbers (*i.e.* $s_i < 50$) up to three years into the cycle causes these large initial estimates of cycle amplitude to be reduced. The timing of the maximum of the cycle is correspondingly adjusted from late 1969 to late 1968.

Figure 8 shows the estimate of maximum smoothed sunspot number $\langle R \rangle_{\max}$ as a function of the time of the last data used for the prediction (blue squares). These estimates are calculated by averaging over 10^5 simulations, as discussed in Section 2.4. The solid black curve is the expected value of $\langle R \rangle_{\max}$ calculated

using all daily data for cycle 20. In this case there are a significant number of days with relatively large sunspot number at the start of the cycle (1965–1966), which cause the initial estimates of $\langle R \rangle_{\max}$ to be larger than that of the mean cycle. However, from mid 1966 onwards there are many days with small sunspot numbers (*i.e.* $s_i < 50$), and few days with large sunspot number (*i.e.* $s_i > \theta(t)$). This causes the forecast to be reduced. The declining phase of cycle 20 (1969–1972) features a significant number of days with large sunspot number, which causes the forecast to increase again. The final estimate of $\langle R \rangle_{\max}$ using all daily sunspot data for cycle 20 is $\langle R \rangle_{\max} = 133 \pm 11$, corresponding to the parameters in Table 5). The observed value of $\langle R \rangle_{\max}$ is 113, which is roughly two standard deviations less than expected, given the data, again illustrating the possible variability in the maximum value.

4. Forecasting the Current Solar Cycle (Cycle 24)

In this section the Bayesian forecasting procedure is applied to forecasting the current solar cycle, cycle 24. There is considerable interest in forecasts for the new cycle given its late start and slow early onset (Russell, Luhmann, and Jian, 2010). In particular the years 2008 and 2009 featured long sequences of days in which the Sun was ‘spotless’ (Tokumaru *et al.*, 2009), and various features of the new cycle have prompted speculation that future activity will be substantially reduced (*e.g.* Livingston and Penn, 2009)

Following Sections 2.2, 2.3, and 2.4, the mean cycle is used as a prior. The start of cycle 24 is taken to be 1 January 2009. With these assumptions the Bayesian estimates of the Fokker–Planck model parameters using all available daily sunspot data 1 January to 31 March 2011 are given in Table 6. The maximum value θ_{\max} of the driver function corresponding to the parameters in Table 6 is 61, which is approximately half the value for the mean cycle. The available data suggests that cycle 24 will be significantly smaller than average.

Figure 9 illustrates the forecasts for cycle 24 following Figures 5 and 7. The daily sunspot numbers for cycle 24 for the interval January 2009 to March 2011 are shown by the green points, and the driver function for the mean cycle is shown by the blue dot-dashed curve. The solid black curve with the largest maximum value is the driver function using the Bayesian estimate of the Fokker–Planck model based on the first year of sunspot data (January 2009 – January 2010), and the second solid black curve uses the first two years of data. Combining the mean cycle prior with the first year of data gives estimates of the driver function very similar to the driver function of the mean cycle. However, due to the large number of days during the latter part of 2010 with small sunspot numbers, the driver function using the first two years of data has a much smaller maximum θ_{\max} than that of the mean cycle. The red dashed curve is the forecast using all data, which has a maximum $\theta_{\max} = 61$.

Figure 10 shows the expected value of $\langle R \rangle_{\max}$ as successively more data are incorporated into the Bayesian prediction method starting from 1 January 2011, following Figures 6 and 8. These (blue squares) estimates are calculated by averaging over 10^5 simulations, as discussed in Section 2.4. The solid black curve is the expected maximum of $\langle R \rangle_{\max}$ for the mean cycle. The early forecasts of $\langle R \rangle_{\max}$ are lower than that of the mean cycle because of the significant number of days during 2009 with zero sunspot number. The forecasts of $\langle R \rangle_{\max}$ steadily increase from early 2009 until mid-2010, but sunspot activity defied expectation and did not significantly increase during the latter part of 2010, and this causes a dramatic reduction in the forecast for $\langle R \rangle_{\max}$ during late 2010 and early 2011. The final estimate using all available data (and matching the parameters in Table 6) is 2009 is $\langle R \rangle_{\max} = 66 \pm 5$. This suggests that cycle 24 will similar in size to cycle 14, and thus larger only than cycles 5 and 6. This prediction is close to the smaller estimates in the literature. For example, Aguirre, Letellier, and Maquet (2008) predicted a smoothed sunspot maximum

of 65 ± 16 , Cameron and Schüssler (2007) predicted a smoothed maximum of 69 ± 15 , and Kakad (2011) a smoothed maximum of 74 ± 10 .

Figure 11 provides a third representation of the forecasts for cycle 24 based on the daily sunspot data for January 2009 to March 2011 (the observed data are shown in blue). The solid red curve is the driver function forecast based on all observed data, matching the Bayesian model estimates in Table 6. From April 2011 to January 2019 the solid red curve provides a basis for prediction of the upcoming sunspot numbers. The two dot–dashed black curves are the upper and lower 1% quantiles for the sunspot number distribution for the forecast, defined by Equation (18). These quantiles show the probability of excursions to large and small daily sunspot numbers. The maximum value attained by the upper 1% quantile is 138 during the period January–March 2013, which may be taken as the most likely time t^* of daily sunspot maximum s^* . The green points are simulated daily sunspot numbers for the remainder of cycle 24 using the Bayesian model estimates in Table 6, with initial condition $s = 66$ on March 31 2011 (the sunspot number observed on that day). In this particular simulation the maximum daily sunspot number is $s^* = 168$ which occurs during October 2012. For the simulation a total of 0.9% and 1.1% of simulated sunspot numbers fall above and below the upper and lower 1% quantiles respectively.

Figure 12 shows the joint distribution of the time t^* and size s^* of daily sunspot maximum for cycle 24, generated using 5×10^5 simulations of daily sunspot number based on the Bayesian estimates in Table 6. Averaging over the simulations we calculate the expected size of the maximum daily sunspot number to be $\langle s^* \rangle = 166 \pm 24$, and this is expected to occur at a time $\langle t^* \rangle$ during March 2013. The sample average daily sunspot number maximum over the previous 13 cycles is $\bar{s}^* = 255$, so on this basis cycle 24 is expected to be significantly smaller than average. The model probability that daily sunspot number maximum for cycle 24 is larger than the average maximum daily sunspot number $\bar{s}^* = 255$ is

$\mathcal{P}(s^* > 255) = 0.4\%$. Hence it is unlikely that individual days with very large sunspot numbers will be observed during cycle 24.

5. Discussion

This paper introduces new techniques for estimating, analysing, and forecasting solar cycles, in particular daily and smoothed sunspot numbers for a cycle, and their statistical properties. In particular, we have shown that even with perfect knowledge of the details of a solar cycle, the observed sunspot maximum (either daily or smoothed) could achieve a broad range of values due to the large fluctuations in the daily sunspot number. This is important for all prediction done a priori, and indicates the true reliability of any forecast of the maximum of a cycle made before the fact.

The main result of this paper is a new Bayesian prediction method for daily sunspot number (Section 2.2). This method is illustrated in application to two dissimilar historical cycles (Section 3), and then is applied to the upcoming solar cycle (Section 4). The method uses as a prior a mean cycle based on the observed solar cycles for 1850–2010 (Section 2.3). Our investigation of this provides a characterisation of solar cycle variability which should also be useful to other workers.

We model the sunspot number as a continuous-time stochastic process, with a probability distribution function described by a Fokker–Planck equation (Noble and Wheatland, 2011). ■

The Bayesian approach to forecasting uses the Fokker–Planck model to include information about solar cycles contained in sunspot data observed up to a given time, and combines these with external information (in principle that provided by precursor or dynamo-based forecasts). The external information is included by specifying an appropriate prior distribution. In this paper we take an historical average solar cycle (a ‘mean cycle’) as a prior, which can be interpreted as a ‘best guess in total ignorance’. However, the methodology can

accommodate any choice of prior. The Bayesian estimation method, combined with the Fokker–Planck equation approach, allows forecasts of the size and shape of the underlying solar cycle, as well as assigning probabilities to the observation of large deviations in sunspot number via calculation of upper and lower quantiles for future sunspot numbers.

In addition, the Fokker–Planck model permits daily sunspot numbers to be simulated over a solar cycle, allowing Monte Carlo construction of the joint distribution of the size and timing of the maximum in daily sunspot number, as well as the distribution of the size of smoothed sunspot maximum $\langle R \rangle_{\max}$. In particular, the distribution of daily sunspot maximum determines the possible size and timing of extreme sunspot numbers during a cycle, which define likely times for the occurrence of intense solar activity. Large flares and coronal mass ejections occurring at these times are drivers of our local space weather (Committee On The Societal and Economic Impacts Of Severe Space Weather Events, 2008). and forecasting of extreme events space weather is an important task (Petrovay, 2010).

The application of the new method to the current solar cycle, cycle 24, provides insight into what we might expect over the next few years. Taking the mean solar cycle as prior and using data for 1 January 2009 to 31 March 2011, the model forecast for the maximum of the smoothed sunspot number is $\langle R \rangle_{\max} = 66 \pm 5$, which is a very low value. The forecast maximum daily sunspot number is 166 ± 24 , expected to occur during March 2013, and this is also very low. These predictions are consistent with other predictions in the literature in suggesting a much smaller than average cycle. The lack of a rapid rise in sunspot number during 2010, in particular, is shown by our modelling to imply a very small upcoming solar cycle.

Acknowledgements We thank Don Melrose for his comments on the manuscript, and an anonymous reviewer whose detailed comments helped improve the paper. P. N. gratefully acknowledges a University of Sydney Postgraduate Scholarship.

References

- Abreu, J.A., Beer, J., Steinhilber, F., Tobias, S.M., Weiss, N.O.: 2008, *Geophys. Res. Lett.* **35**, L20109.
- Aguirre, L.A., Letellier, C., Maquet, J.: 2008, *Solar Phys.* **249**, 103.
- Akaike, H.: 1978, *J. Roy. Stat. Soc. Series D (The Statistician)* **27**(3/4), 217.
- Allen, E.J., Huff, C.: 2010, *Astron. Astrophys.* **516**, A114.
- Bruzek, A., Durrant, C.J. (eds.): 1977, *Illustrated Glossary for Solar and Solar–Terrestrial Physics, Astrophysics and Space Science Library* **69**, 70.
- Cameron, R., Schüssler, M.: 2007, *Astrophys. J.* **659**, 801.
- Committee On The Societal, Economic Impacts Of Severe Space Weather Events: 2008, *Severe Space Weather Events–Understanding Societal and Economic Impacts: A Workshop Report*. Technical report, 4.
- Conway, A.J.: 1998, *New Astron. Rev.* **42**, 343.
- Dacunha-Castelle, D., Florens-Zmirou, D.: 1986, *Stochastics* **19**, 263.
- Dikpati, M., Gilman, P.A.: 2006, *Astrophys. J.* **649**, 498.
- Dikpati, M., de Toma, G., Gilman, P.A.: 2006, *Geophys. Res. Lett.* **33**, L05102.
- Hanslmeier, A., Brajša, R.: 2010, *Astron. Astrophys.* **509**, A5.
- Hathaway, D.H.: 2009, *Space Sci. Rev.* **144**, 401.
- Hathaway, D.H., Wilson, R.M., Reichmann, E.J.: 1994, *Solar Phys.* **151**, 177.
- Hathaway, D.H., Wilson, R.M., Reichmann, E.J.: 1999, *J. Geophys. Res.* **104**, 22375.
- Jaynes, E.T., Bretthorst, G.L.: 2003, *Probability theory: The logic of science*, Cambridge University Press, Cambridge, 149.
- Kakad, B.: 2011, *Solar Phys.* **270**, 393.
- Kane, R.P.: 2002, *Solar Phys.* **209**, 207.
- Kane, R.P.: 2007, *Solar Phys.* **243**, 205.
- Karatzas, I., Shreve, S.E.: 1988, *Brownian Motion and Stochastic Calculus*, Springer–Verlag, New York, 74.
- Letellier, C., Aguirre, L.A., Maquet, J., Gilmore, R.: 2006, *Astron. Astrophys.* **449**, 379.
- Livingston, W., Penn, M.: 2009, *EOS Trans. AGU* **90**, 257.
- Noble, P.L., Wheatland, M.S.: 2011, *Astrophys. J.* **732**, 5.
- Parker, E.N.: 1955, *Astrophys. J.* **121**, 491.
- Pesnell, W.D.: 2008, *Solar Phys.* **252**, 209.
- Petrovay, K.: 2010, *Living Rev. Sol. Phys.* **7**(6).
- Russell, C.T., Luhmann, J.G., Jian, L.K.: 2010, *Rev. Geophys.* **48**, RG2004.
- Sivia, D.: 2006, *Data Analysis: A Bayesian Tutorial*, Second edn. Oxford Science Publications, New York, 6.
- Tokumaru, M., Kojima, M., Fujiki, K., Hayashi, K.: 2009, *Geophys. Res. Lett.* **36**, L09101.

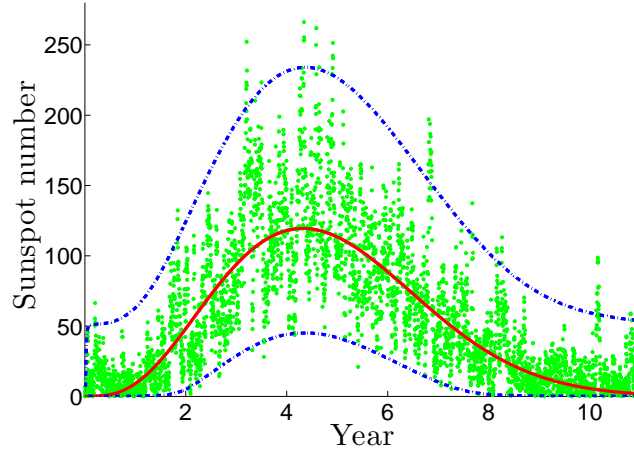


Figure 1. Fokker–Planck modelling of the mean solar cycle, showing the driver function (solid red curve), upper and lower 1% quantiles blue dot–dashed curve), and an example simulation of sunspot numbers (green points), as described in Section 2.4. The maximum value attained by the upper 1% quantile is $s_U(t) = 234$, which occurs 4.3 years after the start of the cycle. In this simulation the maximum of the daily sunspot number is $s^* = 266$, which occurs approximately 4.4 years after the cycle begins.

Waldmeier, M.: 1935, *Astron. Mitt. Eidgen. Sternw. Zurich* **14**, 105.

Yule, G.U.: 1927, *Phil. Trans. Roy. Soc. A* **226**, 267.

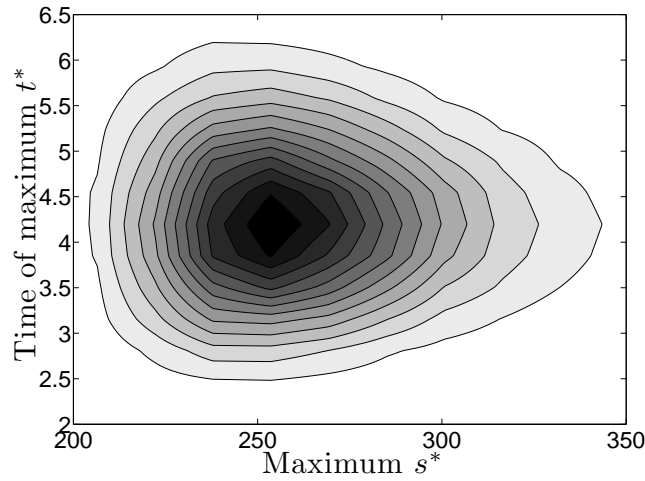


Figure 2. The joint distribution of daily maximum sunspot number s^* and time of maximum t^* for the 5×10^5 Monte Carlo simulations of the mean cycle described in Section 2.4. The expected value of the maximum is 271, which occurs approximately 4.4 years after the start of the cycle. The largest daily maximum value in any simulation is 504, which suggests that the mean cycle has the potential to generate extremely large sunspot numbers, although it is very unlikely.

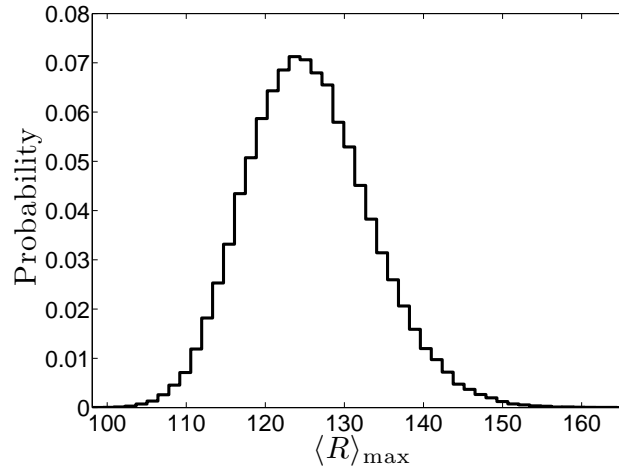


Figure 3. Distribution of the maximum of the 13 month smoothed sunspot number $\langle R \rangle_{\max}$ calculated using 5×10^5 simulations of daily sunspot number for the 'mean cycle' (see Section 2.3). The expected value of the maximum is $\langle R \rangle_{\max} = 125 \pm 8$. The upper and lower 5% quantiles are 113 and 138 respectively.

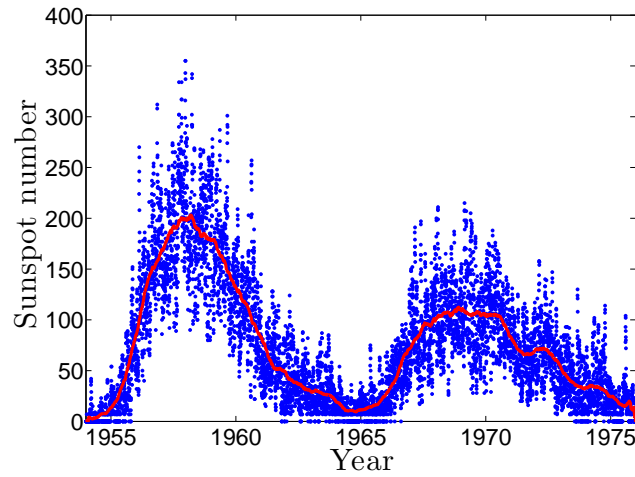


Figure 4. The daily sunspot number observations for cycles 19 and 20 (1954 to 1976) used for forecasting in Section 3. The red curve is a smoothed sunspot number. The maximum of the smoothed sunspot number for cycle 19 is 203, and the maximum for cycle 20 is 113.

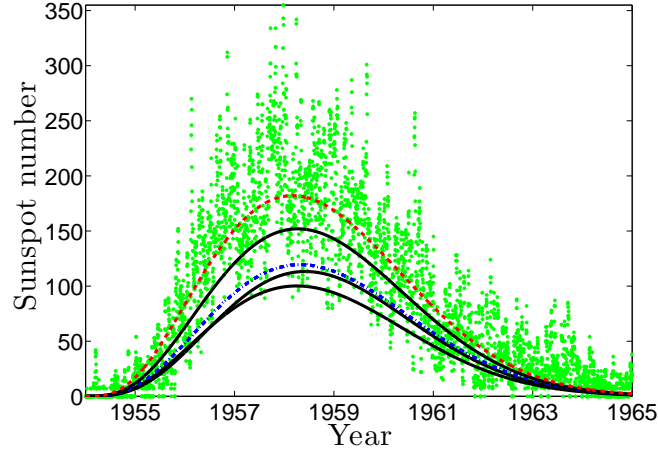


Figure 5. Prediction of cycle 19 using successively more data from the start of the cycle. Daily sunspot numbers for the cycle are shown by the green points. The driver function for the mean cycle prior which uses no sunspot data is in blue (dot–dashed), and the Bayesian estimate using all sunspot data for 1954 to 1964 is the red dashed curve. The model parameters for the red curve are given in Table 4. The solid black curve with the smallest maximum value is the forecast using ten days of data, the next smallest uses one year of data, and the largest solid black curve uses two years of data.

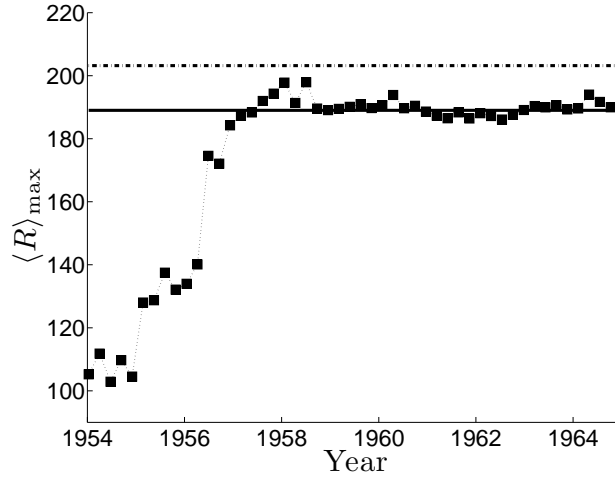


Figure 6. Prediction of cycle 19 using successively more data from the start of the cycle. The value of the maximum $\langle R \rangle_{\max} = 203$ for the observed cycle 19 data is shown by the dot–dashed line. The expected value of $\langle R \rangle_{\max}$ calculated by average over 10^5 cycles is $\langle R \rangle_{\max} = 189$, and is shown by the solid line. The forecasts of $\langle R \rangle_{\max}$ for the Bayesian modal estimate using daily sunspot up to the indicated time, and calculated by averaging over 10^3 simulations are shown by the squares. From 1955 to 1957 the forecast of $\langle R \rangle_{\max}$ rises rapidly and then is approximately constant. The final value, matching the parameters in Table 4, is $\langle R \rangle_{\max} = 182$.

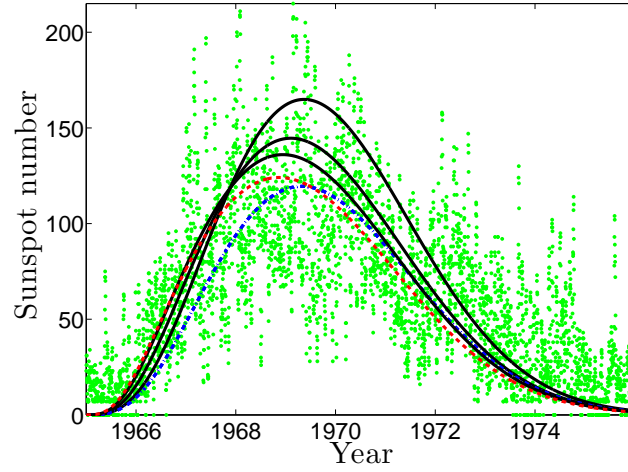


Figure 7. Prediction of cycle 20 using successively more data from the start of the cycle. Daily sunspot numbers for the cycle are shown in green. The driver function for the mean cycle prior which uses no sunspot data is the blue dot-dashed curve, and the Bayesian estimate using all sunspot data for 1965 to 1975 is shown by the red dashed curve. The model parameters for the red dashed curve are given in Table 5. The black solid curve with the largest amplitude is estimated using ten days of data, the next largest uses one year of data, and the largest solid black curve uses two years of data respectively.

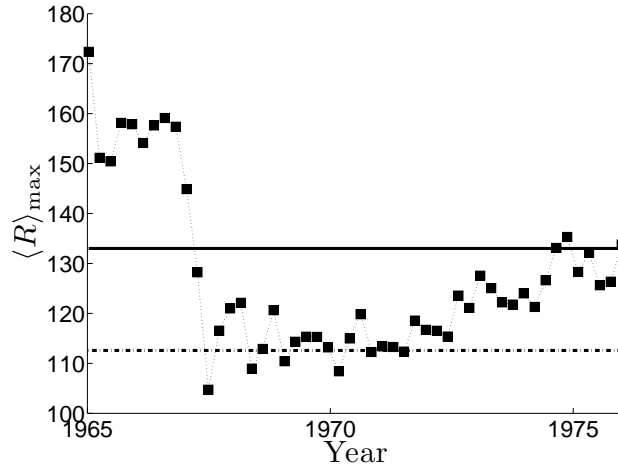


Figure 8. Prediction of cycle 20 using successively more data from the start of the cycle. The value of the maximum $\langle R \rangle_{\max} = 113$ for the observed cycle 20 data is shown by the dot-dashed line. The expected value of $\langle R \rangle_{\max}$ calculated by averaging over 10^5 simulations is $\langle R \rangle_{\max} = 133$, shown by the solid line. The forecasts of $\langle R \rangle_{\max}$ for the Bayesian modal estimate using daily sunspot data up to the indicated time, and calculated by averaging over 10^3 simulations are shown by the squares. The significant number of large sunspot numbers at the start of the cycle cause early estimates of $\langle R \rangle_{\max}$ to be larger than expected. However, the lack of large sunspot numbers during solar maximum cause estimates of $\langle R \rangle_{\max}$ to be reduced. The large variation in daily sunspot number causes estimates of $\langle R \rangle_{\max}$ to slowly rise to the final value ($\langle R \rangle_{\max} = 133$), matching the parameters in Table 5.

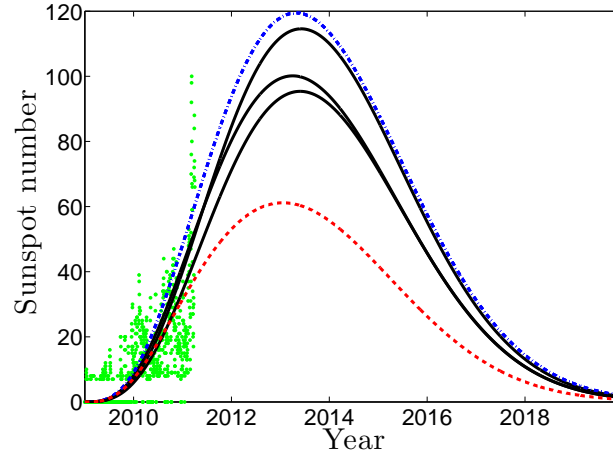


Figure 9. Prediction of cycle 24 using successively more data from the start of the cycle. Sunspot data for the cycle are shown by the green points. The driver for the mean cycle prior which uses no sunspot data is shown by the blue dot-dashed curve, and the driver function for the Bayesian estimates using all available data for the cycle (January 2009 to March 2011) is shown by the red dashed curve. The solid black curve with the largest maximum value is the forecast for the driver function using one year of daily sunspot data from the start of the cycle, and the second solid black curve uses two years of data.

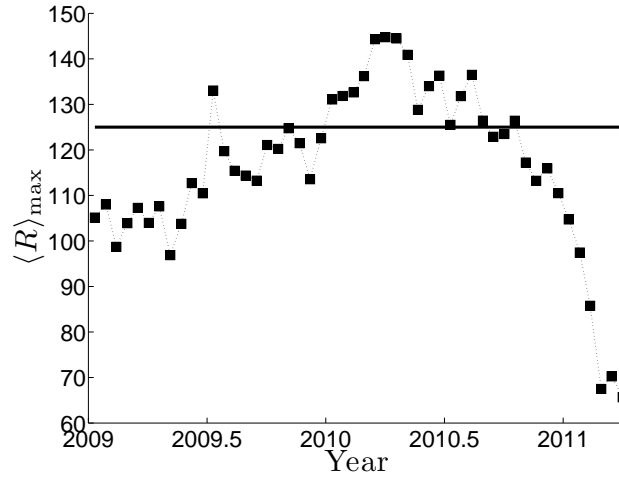


Figure 10. Prediction of cycle 24 using successively more data from the start of the cycle. The expected maximum $\langle R \rangle_{\max} = 125$ for the mean cycle is shown by the solid line. The forecasts of $\langle R \rangle_{\max}$ for the Bayesian modal estimate using daily sunspot data up to the indicated time, and calculated by averaging over 10^3 simulations are shown by the squares. The lack of large sunspot numbers in late 2010 causes a dramatic reduction in the expected size of $\langle R \rangle_{\max}$. The final value, matching the parameter estimates in Table 6, is $\langle R \rangle_{\max} = 66$.

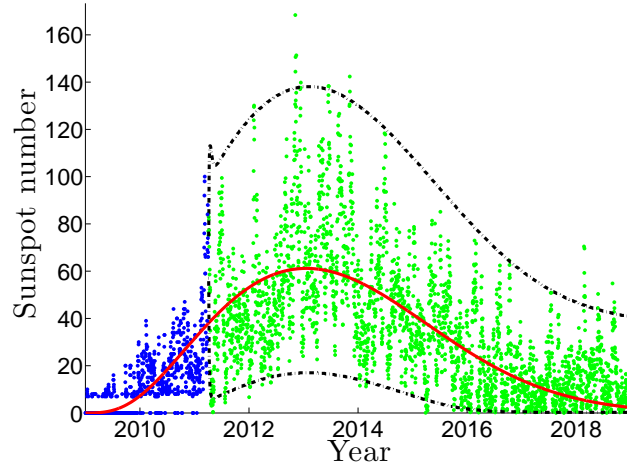


Figure 11. Prediction of cycle 24: illustration of the forecast distribution of daily sunspot numbers for the remainder of cycle 24. The model parameters used in the forecast are the Bayesian estimates given in Table 6. The solid red curve is the forecast of the driver function, and the two dot-dashed black curves are the upper and lower 1% quantiles for the sunspot number distribution. The blue points are the daily sunspot numbers observed for January 2009 to March 2011 used for the prediction. The green points are a simulation of future sunspot numbers using the parameters in Table 6. The upper quantile attains a maximum value of 138 during the period January–March 2013, identifying this as the most likely time for a maximum in the daily sunspot numbers.

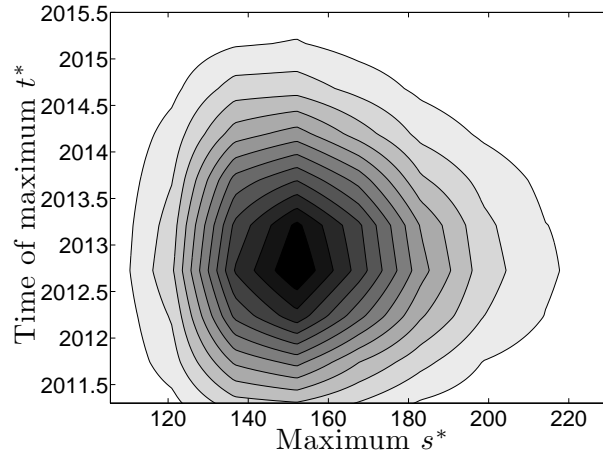


Figure 12. The joint distribution of sunspot maximum s^* and time of maximum t^* for a sequence of 5×10^5 Monte Carlo simulations of solar cycle 24, as described in Section 4. The simulation uses the Bayesian model parameters in Table 6, and the initial condition $s_0 = 66$. The expected size of the daily sunspot maximum is 166 ± 24 , which is most likely to occur around March 2013.

Table 1. Maximum likelihood estimates of the parameters $\Omega = [a, b, c, \kappa, \beta_0, \beta_1, \beta_2]$ for the previous 13 solar cycles over the interval 1850 to 2010.

Cycle	\hat{a} [day ⁻³]	\hat{b} [day]	\hat{c}	$\hat{\kappa}$ [day ⁻¹]	$\hat{\beta}_0$ [day ⁻¹]	$\hat{\beta}_1$ [day ⁻¹]	$\hat{\beta}_2$ [day ⁻¹]
23	7.8234×10^{-8}	1514.8	0.22174	0.08555	17.689	1.6569	2.1862×10^{-5}
22	14.112×10^{-8}	1368.2	0.33153	0.07305	22.361	1.6302	1.1872×10^{-3}
21	12.497×10^{-8}	1414.0	0.48998	0.07325	22.069	1.4652	3.0413×10^{-3}
20	7.2861×10^{-8}	1450.4	0.90401	0.06151	44.288	1.1235	1.2022×10^{-3}
19	14.048×10^{-8}	1391.4	0.66332	0.07994	18.636	1.8863	7.3281×10^{-7}
18	10.592×10^{-8}	1411.5	0.65807	0.09238	22.541	2.3351	1.6617×10^{-4}
17	7.2515×10^{-8}	1440.4	0.80478	0.11587	30.236	1.7644	7.4863×10^{-3}
16	5.1614×10^{-8}	1457.8	0.43823	0.13072	14.619	2.8419	4.0631×10^{-3}
15	7.8341×10^{-8}	1285.2	0.83355	0.10493	23.245	3.4815	2.8562×10^{-3}
14	3.5130×10^{-8}	1576.8	0.42673	0.12617	10.136	3.5719	8.5559×10^{-4}
13	8.5060×10^{-8}	1256.3	0.81241	0.13579	24.716	3.3131	2.4606×10^{-4}
12	3.7627×10^{-8}	1526.9	0.55401	0.12793	14.543	3.2136	2.1382×10^{-4}
11	9.7135×10^{-8}	1356.6	0.73723	0.17509	40.229	4.5763	9.1951×10^{-4}

Table 2. Sample means $\bar{\Omega}$ for each model parameter estimated for the last 13 cycles. The solar cycle with $\Omega = \bar{\Omega}$ is the mean solar cycle.

\bar{a} [day ⁻³]	\bar{b} [day]	\bar{c}	$\bar{\kappa}$ [day ⁻¹]	$\bar{\beta}_0$ [day ⁻¹]	$\bar{\beta}_1$ [day ⁻¹]	$\bar{\beta}_2$ [day ⁻¹]
8.6233×10^{-8}	1419.3	0.60582	0.10633	23.486	2.5277	1.7123×10^{-3}

Table 3. Correlation matrix for the model parameters estimated for the previous 13 solar cycles 1850–2010.

	a	b	c	κ	β_0	β_1	β_2
a	1.0000	-0.5268	-0.0243	-0.4671	0.2148	-0.4035	-0.1543
b		1.0000	-0.5270	-0.0842	-0.3877	-0.1800	-0.0196
c			1.0000	0.1596	0.6627	0.1721	0.2069
κ				1.0000	-0.0022	0.8945	0.0733
β_0					1.0000	-0.0921	0.1380
β_1						1.0000	-0.1706
β_2							1.0000

Table 4. Bayesian parameter estimates for solar cycle 19 using the mean cycle as a prior and including data for the entire cycle.

\hat{a} [day ⁻³]	\hat{b} [day]	\hat{c}	$\hat{\kappa}$ [day ⁻¹]	$\hat{\beta}_0$ [day ⁻¹]	$\hat{\beta}_1$ [day ⁻¹]	$\hat{\beta}_2$ [day ⁻¹]
13.23×10^{-8}	1401	0.6929	0.0766	18.74	1.891	3.751×10^{-7}

Table 5. Bayesian parameter estimates for solar cycle 20 using the mean cycle as a prior and including data for the entire cycle.

\hat{a} [day ⁻³]	\hat{b} [day]	\hat{c}	$\hat{\kappa}$ [day ⁻¹]	$\hat{\beta}_0$ [day ⁻¹]	$\hat{\beta}_1$ [day ⁻¹]	$\hat{\beta}_2$ [day ⁻¹]
8.2605×10 ⁻⁸	1400.5	0.8894	0.05624	40.219	1.0995	1.621×10 ⁻³

Table 6. Bayesian parameter estimates for solar cycle 24, using the mean cycle as a prior and including all sunspot data from 1 January 2009 to 31 March 2011.

\hat{a} [day ⁻³]	\hat{b} [day]	\hat{c}	$\hat{\kappa}$ [day ⁻¹]	$\hat{\beta}_0$ [day ⁻¹]	$\hat{\beta}_1$ [day ⁻¹]	$\hat{\beta}_2$ [day ⁻¹]
4.2962×10 ⁻⁸	1400.0	0.7804	0.09514	10.487	1.6496	0.0040